Principles of Ion Selection, Alignment, and Focusing in Tandem Ion Mobility Implemented Using Structures for Lossless Ion Manipulations (SLIM)

Rachel M. Eaton, Samuel J. Allen, Matthew F. Bush*

Original manuscript submitted to the *J. Am. Soc. Mass Spectrom.* on January 16, 2018

Revised manuscript submitted to the *J. Am. Soc. Mass Spectrom.* on February 20, 2018

Address reprint requests to:

Matthew Bush, (206) 543-7835, mattbush@uw.edu

University of Washington, Department of Chemistry, Box 351700

Seattle, WA 98195-1700

*Address correspondence to mattbush@uw.edu

Abstract

Tandem ion mobility (IM) enables the characterization of subpopulations of ions from larger ensembles, including differences that cannot be resolved in a single dimension of IM. Tandem IM consists of at least two IM regions that are each separated by an ion selection region. In many implementations of tandem IM, ions eluting from a dimension of separation are filtered and immediately transferred to the subsequent dimension of separation (selection-only experiments). We recently reported a mode of operation in which ions eluting from a dimension are trapped prior to the subsequent dimension (selection-trapping experiments), which was implemented on an instrument constructed using the Structures for Lossless Ion Manipulations (SLIM) architecture. Here, we use a combination of experiments and trajectory simulations to characterize aspects of the selection, trapping, and separation processes underlying these modes of operation. For example, the actual temporal profile of filtered ions can be very similar to the width of the waveforms used for selection, but depending on experimental parameters, can differ by up to ±500 μs. Experiments and simulations indicate that ions in selection-trapping experiments can be spatially focused between dimensions, which removes the broadening that occurred during the preceding dimension. During focusing, individual ions are thermalized, which aligns and establishes common initial conditions for the subsequent dimension. Therefore, selection-trapping experiments appear to offer significant advantages relative to selection-only experiments, which we anticipate will become more pronounced in future experiments that make use of longer IM separations, additional dimensions of analysis, and the outcomes of this study.

Introduction

A variety of techniques are available to probe the interactions and assembly of biomolecules. Many techniques such as x-ray diffraction or cryogenic electron microscopy provide high resolution images of molecules, but require or benefit from restricting molecules to single, static conformations during the experiment [1, 2]. Native mass spectrometry (MS) uses aqueous solutions at biologically relevant pH and soft ionization methods to minimize the disruption of solution-phase interactions during gas-phase analysis [3]. Native MS often provides data that is complementary to condensed-phase measurements. For example, negative-stain electron microscopy and native MS experiments were used to determine the stoichiometry and spatial arrangement of the subunits comprising the Cascade ribonucleoprotein complex [4].

The addition of ion mobility (IM) to native MS enables the separation and near-simultaneous characterization of multiple structural conformers of a biomolecule or biomolecular complex [5–8]. IM is a gas-phase electrophoretic technique that uses an electric field to rapidly separate ions in a neutral gas based on differences in their shape and charge [9–11]. However, the conformational heterogeneity of protein ions, rather than the resolving power or accuracy of the instrument, limits the quality of the data in most experiments [12, 13]. Tandem IM improves upon one-dimensional IM by enabling the isolation of structural conformations prior to an additional IM separation. Tandem IM consists of at least two IM regions that are each separated by an ion selection region; the IM regions can disperse ions in time [12, 14–18], field [19], or space [17, 20] depending on the design of the instrument. Most ion selection methods use time-dependent, voltage-controlled gates to selectively transmit ions of a desired mobility by destabilizing the trajectories of ions that arrive at different times [15, 21]. Previously, ion gating has been performed using grid mesh electrodes [21], Bradbury-Nielsen gates [22, 23], or the

voltage bias between two adjacent ion funnels [24]. There are also examples of trapping ions between dimensions of IM [24, 25]. Tandem IM has been used to study the stability of structural subpopulations, demonstrating that protein ions in the gas phase have conformational subpopulations that are unresolved in one-dimensional IM [12, 26, 27]. Additionally, structural subpopulations analyzed by tandem IM may retain a "memory" of structural conformations that existed in solution [18, 25].

Recently, the Structures for Lossless Ion Manipulations (SLIM) architecture [28] was used to create a tandem IM instrument. Between the IM dimensions of that instrument, subpopulations are selected in a time-dependent fashion by diverting other ions off of the axis of transmission and onto a secondary pathway towards a collection electrode [25]. SLIM devices consist of mirrored pairs of printed circuit boards that are patterned with sets of electrodes to generate electric fields that control ion movement [29–31]. In this implementation, DC ± RF potentials are applied to create an electrostatic drift field that mimics RF-confining drift cells [29, 32, 33]. Ion selection uses a tee in which two intersecting sets of electrodes create a collinear and an orthogonal path from the incidental linear path [30]. Independently controlled voltages applied to electrodes located at the intersection of the two paths enable control of the ion path. By manipulating the potentials on these electrodes as a function of time, ions are diverted from the collinear and onto the orthogonal path, enabling mobility-based sorting of ions [25, 34, 35]. In these tandem IM experiments, ion selection is followed by a separate trapping region [25]. Ion trapping is achieved by applying independently controlled DC potentials to electrically isolated boards [25, 36] to inhibit ion transmission. Discrete ion selection and trapping elements in this instrument enable multiple modes of tandem IM.

We recently used this implementation of tandem IM to probe the dynamics of native-like cytochrome *c* ions trapped at ambient temperatures for up to ~33 seconds [25]. This implementation used uniform drift fields to enable the direct determination of the mobilities of the ions in each dimension [33], *i.e.*, before and after trapping. These tandem IM experiments demonstrated ion isolation and trapping of subpopulations of protein ions. Here, we characterize the selection and trapping processes underlying those experiments. Understanding the factors that affect tandem IM experiments using SLIM will help improve future analyses of the structural stability and heterogeneity of native-like biomolecules so that these methods can be applied to differentiate similar biomolecules.

Methods

Experimental Overview

The instrument used for these experiments (Figure 1A) has been described previously [25, 33]. $[GRGDS+H]^+$ ions were generated using electrokinetic nanoelectrospray ionization [37] from solutions containing 0.1 mg mL^{-1} GRGDS (490 Da, Waters Corporation 700005089) in a 49.5/49.5/1 (v/v) mixture of water, acetonitrile, and formic acid. Ions from electrospray were introduced into the first vacuum chamber, where they were accumulated in an ion funnel trap [38]. Lowering the potential of two of the grid electrodes in the ion funnel trap releases a packet of ions (Figure 2) into the second vacuum chamber, which contains an ion funnel with a rectangular cross section [39], an ion mobility drift region, and an ion funnel with a circular cross section [40, 41] (Figure 1A). The first and second chambers were operated at pressures of 3.98 and 4.04 Torr nitrogen gas, respectively, which was maintained by controlling the conductances to a vacuum pump and introducing 5 mL min^{-1} of N_2 gas (standard temperature and pressure)

into the second chamber. The drift fields in the post-trapping region of the ion funnel trap, the rectangular ion funnel, and the circular ion funnel were 14, 4, and 6 V cm^{-1}, respectively. The ion mobility drift region was constructed using the SLIM architecture (Figures 1B and 1E), in which planar electrodes are deposited directly onto printed circuit boards that apply DC ± RF potentials [29–31]. Pairs of electrode-facing, 7.62 x 7.62 cm boards, with a 3.97 mm board-to-board distance, form modules that were combined to enable the tandem IM experiments described here (Figure 1B). After the circular ion funnel, ions were analyzed using a Waters Q-Tof Premier mass spectrometer and an independent analog-to-digital converter (ADC, Keysight Technologies Acqiris U1084A, Santa Rosa, CA), as described previously [33].

Tandem IM

Ions were first accumulated and then released from an ion funnel trap, as described previously [38, 41]. To accumulate and trap ions, the trap grid and exit grid in the ion funnel trap were increased by 4 and 32 V, respectively, relative to the preceding ion funnel electrode. These potentials were reduced for 375 μs to inject ions for IM separation (Figure 2). Ions pass through three linear modules prior to entering the tee module (position 4, Figure 1B). The boards comprising this module contain a linear array of electrodes (the collinear path) to transmit ions along the path to the mass analyzer, and an orthogonal array of electrodes (the orthogonal path) to divert ions away from the mass analyzer (Figure 1F) [34, 35, 42]. Mobility filtering is performed by applying time-dependent DC potentials to the "switch guard" and "switch rung" electrodes near the intersection of the collinear and orthogonal paths (Figure 1B and 1F). To transmit ions along the collinear path, the switch rung and guard were raised to +11 V relative to the switch region. To divert ions down the orthogonal path, the switch rung was lowered to 0 V

and switch guard raised to +16 V relative to the switch region. Ions in the orthogonal path will experience a drift field of 6 V cm^{-1}. The time during which the switch electrodes were programmed to transmit ions will be referred to as the "programmed window" (Figure 2).

Tandem IM was performed using "selection-only" and "selection-trapping" modes of operation. In both modes, ions are separated in the first dimension of IM (^{1}D), which includes all transfer funnels and SLIM modules prior to the switch region. For "selection-only" experiments, ions of interest are selectively transmitted through the tee and then immediately enter the second dimension of IM (^{2}D, Figure 1C). The use of ^{1}D and ^{2}D to represent the first and second dimensions of a multidimensional separation is common in the chromatography community [43]. In "selection-trapping" experiments, ions are selected in the tee region and accumulated in the "junction trap" immediately prior to module 5 (Figure 1B). Independent DC voltage control was enabled at the output of module 4 and the input of module 5; trapping was performed by elevating the input DC voltage of module 5 above the output DC voltage of module 4 (Figure 1B). The bias between those two points will be referred to as the "applied trap height". The applied trap height was decreased to release the accumulated ions into ^{2}D (Figure 1D), and then raised again just prior to the next ion packet arriving at the switch. In both modes, ^{2}D includes both the remaining SLIM modules and the final ion funnel. A summary of the time-dependent potentials used in these experiments is shown in Figure 2.

Determining Ω Values using SLIM

Ions are separated using a constant DC gradient; no traveling waves are used in this implementation of SLIM. As validated previously [33], the drift velocity (v_D) of ions under these conditions depends on their mobility (K) and the applied electric field (E):

$$v_{\mathrm{D}} = KE \quad (1)$$

Measurements were conducted as a function of E to determine K values and the transport times outside the SLIM drift region (t_0). Ω values were then determined using the Mason-Schamp equation [44]:

$$\Omega = \frac{3ez}{16N}\left(\frac{2\pi}{\mu k_{\mathrm{B}}\mathrm{T}}\right)^{1/2}\frac{1}{K} \quad (2)$$

where e is the elementary charge, z is the ion charge state, N is the drift-gas number density, μ is the reduced mass of the ion and drift gas (N_2), k_{B} is the Boltzmann constant, and T is the drift-gas temperature of 300 K.

Ion Trajectory Simulations

Ion trajectories were simulated in SIMION 8.1 [45] using electrode dimensions reported previously [33], 4 Torr N_2 gas, and an estimate of the mean free path based on a previously reported Ω value for $[GRGDS+H]^+$ [46]. For trajectories used to characterize ions stored in a junction trap, the HS1 hard sphere approximation was used with previously reported methods [25, 32]. To characterize ion selection, trajectories were simulated using Stokes law dampening. The potentials applied to electrodes mimicked those applied during the corresponding experiments, except that ions in the orthogonal path will experience a drift field of 20 V cm^{-1} (whereas ions in the experiments will experience a field of 6 V cm^{-1} in that region). At the start of each ion trajectory, the switch region was programmed to divert ions. After some initial time, the switch guard and switch rung electrodes were set to transmit ions (t_{transmit}; Figure S1A) for the duration of the programmed window. Immediately after the programmed window (t_{divert}; Figure S1A), these electrodes were set to divert ions again. Ion trajectories for each programmed window were performed as a function of the starting position upstream of the switch region

(Figure S1). The starting positions were selected based on the expected positions of the ion after every 7 μs of drift given the conditions in the collinear region. Using this approach and holding $t_{transmit}$ constant was easier to implement than using a constant starting position and varying $t_{transmit}$, but is expected to provide similar information. The final position of the ion was recorded and used to determine whether the ion was diverted or transmitted.

Results and Discussion

The objective of this study is to understand the factors that affect the selection and trapping processes underlying a recently reported instrument for IM-IM-MS [25] that made use of the Structures for Lossless Ion Manipulations (SLIM) architecture. Two operational modes were evaluated for that implementation of tandem IM. In selection-only experiments, ions are separated using the first and second IM dimensions (^{1}D and ^{2}D, Figure 1C). The switch region in between these two IM dimensions is used to selectively transmit subpopulations of ions. In selection-trapping experiments, ions that are selectively transmitted from ^{1}D are transferred to a junction trap (Figure 1D); this junction trap was used to accumulate and store ions prior to ^{2}D. The time required to reach the switch region depends on the mobility of the ion. Therefore, in both operational modes, the same $t_{transmit}$ and t_{divert} were used to isolate ions at the end of ^{1}D (Figure 2).

$[GRGDS+H]^+$ was selected to evaluate these tandem IM experiments because the arrival-time distributions measured using other IM instruments are consistent with a single, gas-phase structure (Figure S2). Thus, experimental peak widths of $[GRGDS+H]^+$ will be sensitive to any additional contributions to broadening beyond diffusion and gating [13]. The peak width of a single conformer of $[GRGDS+H]^+$ was estimated from the initial width of the ion packet (375

μs), and diffusion of the ions during IM and any other subsequent analysis. The width at the base of this distribution was estimated using this equation for the separation of a single-conformer ion [47, 48]:

$$w_{\text{conformer}}^2 = w_{\text{gate}}^2 + \sum {w_{\text{diff}}}^2 = w_{\text{gate}}^2 + \sum_n \frac{32 k_B T}{ezV_n} \left(\frac{{L_n}^2}{KV_n}\right)^2 \quad (3)$$

where V_n is the drift voltage and L_n the drift length of each of n drift regions in the instrument after gating. The drift regions included in this calculation will depend on the experiment; the widths at base estimated for each drift region are summarized in Table S1. K was calculated using the collision cross section value for $[GRGDS+H]^+$ reported previously [46]. For these tandem IM experiments, the gating term will be used to represent the ion trapping or filtering that affects the initial temporal width of the ion packet.

Results from Selection-Only Tandem IM

To evaluate selection-only tandem IM experiments, the full population of $[GRGDS+H]^+$ ions generated by electrospray ionization was compared to two subpopulations. For these experiments, the collinear drift field and switch guard voltages during ion diversion were kept constant at 6 V cm^{-1} and +16 V relative to the switch region, respectively. The entire $[GRGDS+H]^+$ distribution was transmitted from ^1D to ^2D by deactivating the switch from 32.00 (t_{transmit}) to 36.375 (t_{divert}) ms relative to the beginning of ion injection (Figure 2). This created a 4.375 ms programmed window during which the ions could pass through the switch region and onto the ^2D (Figure 1C). Two different temporal regions of the entire distribution were selected by transmitting drift times 33.250 to 33.750 and 34.625 to 35.125 ms (0.500 ms programmed windows). To enable direct comparisons of the arrival-time distributions resulting from these three experiments, the residence times of ions in ^2D (the ^2D time) were calculated:

$$^2D\ time = t_{\text{measured}} - \frac{t_{\text{transmit}} + t_{\text{divert}}}{2} - t_0 \quad (4)$$

where t_{measured} is the arrival-time at the detector relative to when ions were released from the ion funnel trap and t_0 is the transport time of ions from the end of ^{2}D to the detector (*i.e.*, the residence time inside the attached Q-Tof Premier instrument). The value for t_0 was determined from *E*-dependent measurements. Figure 3A shows the ^{2}D times for the three populations characterized using these selection-only experiments.

The experimental distributions were characterized using the observed width at base (w_{obs}), which was determined from 4σ of the normal distribution that has the smallest root mean square deviation with the experimental distribution. The experiments using a 4.375 ms programmed window yielded w_{obs} of 3.5 ms that is similar to, albeit slightly wider than, that expected for a single conformer that was released from the ion funnel trap (w_{gate} = 0.375 ms) and underwent diffusion along ^{1}D and ^{2}D ($w_{\text{conformer}}$ = 3.0 ms). Both experiments using 0.500 ms programmed windows yielded distributions (w_{obs} = 1.8 ms) that are narrower than the preceding w_{obs} or $w_{\text{conformer}}$ values. In contrast, that w_{obs} value is similar to that calculated assuming w_{gate} = 0.500 ms and diffusion through ^{2}D ($w_{\text{conformer}}$ =1.8 ms). The similarities in those widths are consistent with both subpopulations of $[GRGDS+H]^+$ consisting of a single conformer. The observed and expected distributions of each selected population are summarized in Table 1.

Narrower programmed windows filter away much of the diffusional broadening that occurs during ^{1}D, resulting in narrower distributions at the detector after ^{2}D. In Figure 3A, the distributions for the two subpopulations are similar to each other, but appear at shorter ^{2}D times than the distribution of the full population. The difference in the ^{2}D times for the subpopulations versus the full populations can be attributed to bias caused by the corrections introduced using Equation 4. Briefly, if ions eluting from ^{1}D are not well centered between t_{transmit} and t_{divert}, the

resulting ^{2}D times may be biased, which demonstrates a challenge in interpreting the results for different populations obtained using selection-only tandem IM experiments.

Effects of the Programmed Window

To investigate the effect of the programmed window on the width of peaks in selection-only mode, $[GRGDS+H]^{+}$ was analyzed as a function of the width of the programmed window, using the same collinear drift field and switch guard voltage as the preceding experiments. The intensity of the transmitted ions increases by two orders of magnitude as the programmed window is increased from 250 to 2000 μs, with a more modest increase as the programmed window is increased from 2000 to 16000 μs (Figure 4). Since the midpoint of each programmed window was optimized to be near the centroid of the $[GRGDS+H]^{+}$ peak from ^{1}D, it is intuitive that the greatest gains in intensity come from the initial widening of the programmed window.

The w_{obs} values of these distributions are plotted in Figure 4. These values are then compared with $w_{conformer}$, calculated assuming that w_{gate} equals the width of the programmed window and diffusion along ^{2}D. The w_{obs} and $w_{conformer}$ values are similar for short programmed windows. The w_{obs} values increase with increasing programmed window until the transmitted ion packet is no longer limited by the width of the programmed window (~4000 μs). That is, the relative contributions from the programmed window will increase with that parameter until w_{obs} is instead limited by the width of the distribution eluting from ^{1}D.

Which Ions are Actually Transmitted?

The preceding analysis assumed that the temporal width of the ion packet entering ^{2}D was equal to the width of the programmed window, which Figure 4 shows may not be valid

under all conditions. To assess that assumption, including the effects of the collinear drift field and the switch guard voltage used to divert ions, ion trajectories in the tee module were simulated as described in the *Methods* section. Representative trajectories are shown in Figure S1. Ions that arrive in the switch region before the switch is deactivated (Figure S1B) or after the switch is reactivated (Figure S1D) were diverted to the orthogonal path and not transmitted. Ions that arrive in the switch region while it is deactivated (Figure S1C) or whose trajectories are not sufficiently diverted by the switch region (Figure S1B and S1D), are transmitted. As a consequence of the design of the simulations, each trajectory corresponds to 7 μs of the incident beam. Therefore, the actual window of transmitted ions (w_{actual}) is the product of 7 μs and the number of transmitted trajectories, which depends on the potentials applied to electrodes during the simulations. Although the drift field along the orthogonal path in these simulations (20 V cm^{-1}) is greater than that used in the preceding experiments (6 V cm^{-1}), we expect that the trends in the simulations should provide insights into the experiments.

Figure 5A shows w_{actual} as a function of programmed windows ranging from 50 to 2000 μs at collinear drift fields of 4, 6, or 8 V cm^{-1}. The selection efficiency is defined as the ratio of w_{actual} to the programmed window; the solid grey line in Figure 5 corresponds to a selection efficiency of unity. Selection efficiency decreases with collinear drift fields, *e.g.*, at a 4, 6, and 8 V cm^{-1} a programmed window of 500 μs yields w_{actual} values of 21, 476, and 770 μs, respectively. Interestingly, for 8 V cm^{-1} the selection efficiency is greater than unity for all programmed windows considered. High fields along the collinear axis enable continued transmission of ions through the switch region despite the contributions from fields in the orthogonal direction. Depending on how close the ion is to the end of the switch region and the

field along the collinear path, some partially diverted ions may be transmitted, which results in larger w_{actual} values and increased selection efficiency.

The effects of varying switch guard voltages on the selection efficiency is shown in Figure 5B. The selection efficiency decreases with increasing switch guard voltage, *e.g.*, using a programmed window of 500 µs and switch guard voltages of +16, +36, and +56 V yields w_{actual} values of 476, 175, and 0 µs, respectively. This decrease is attributed to increased field penetration in the switch region by the higher switch guard potentials, which results in more efficient diversion of ions to the orthogonal path. At high switch guard voltages, only ions on the edge of the switch region will avoid diversion when the switch guard is active. Since the width of the programmed window affects the number of transmitted ions, changes in the selection efficiency will affect the sensitivity and selectivity in selection-only and selection-trapping experiments.

Results from Selection-Trapping Tandem Ion Mobility

In selection-trapping mode, the ions transmitted from ^{1}D are first accumulated in the junction trap (Figure 1B). The junction trap was established by biasing the beginning of module 5 relative to the end of module 4 by the "applied trap height", *e.g.*, Figure 6A shows the DC potential at the surface of the boards near the interface of the two modules. The period after selection during which the junction trap accumulates and stores ions will be referred to as the "delay time". A common delay time of 3.8 ms was used for all selection-trapping experiments (Supporting Information Figure S3) in order to ensure all selected ions are transferred and accumulated in the junction trap, while also minimizing residence time in that trap. After the delay time, ions were released from the junction trap and separated along ^{2}D.

The ^{2}D times in selection-trapping experiments are calculated by subtracting t_0 from $t_{measured}$ (Figure 2). Figure 3B shows ^{2}D times in selection-trapping mode are shorter than those from selection-only mode (Figure 3A) using the same programmed windows. This is attributed to the shorter length of ^{2}D in selection-trapping experiments (see Figures 1C and 1D). The distributions resulting from all three programmed windows are similar to each other. That is, as a consequence of accumulating ions in the junction trap prior to ^{2}D, differences in the programmed windows used for ion selection do not carry over or bias the ^{2}D times. The w_{obs} values for these distributions (1.7 to 1.8 ms, Table 1) are slightly larger than calculated for a single conformer assuming no contributions from gating (w_{gate} = 0 ms) and diffusion along ^{2}D ($w_{conformer}$ = 1.5 ms). The small differences between these w_{gate} and $w_{conformer}$ values, as well as the appropriateness of assuming no contributions from gating, will be discussed in the following section.

Effective Trap Height and Spatial Distribution of Ions During Junction Trapping

In order to characterize the effects of drift field and applied trap height on selection-trapping experiments, ion trajectories were simulated using drift fields of 4, 6, or 8 V cm^{-1} with an applied trap height of +12 V as well as applied trap heights of +10, +12, or +14 V with a drift field of 6 V cm^{-1}. These conditions are all adequate to accumulate and trap incident ions over the time scales of the simulations and in selection-trapping experiments. The electrostatic potential along the axis of transmission (the rotational axis of symmetry along z) for these conditions is shown in Figure 6B. Each potential exhibits a local minimum that is prior to the interface between the two modules, which is the origin of the axis. The effective trap height, which was calculated by subtracting the potential at the local minimum (V_{min}) from the potential at the local

maximum (V_{max}) near the interface between the two modules, is plotted in Figure 6C. These values are systematically lower than the corresponding applied trap height because of the superimposed drift field. Increasing the applied trap height from +10 to +14 V, while holding the drift field at 6 V cm^{-1}, increases the effective trap height from to 5.2 to 8.4 V. Conversely, increasing the drift field from 4 to 8 V cm^{-1} with an applied trap height of +12 V decreases the effective trap height from 7.8 to 5.9 V.

The effective drift length, which is used to calculate K and Ω values determined from ^{2}D times, will depend on the location of ions as they are released from the junction trap. To characterize the location of ions in a junction trap, single ion trajectories were simulated using the HS1 hard sphere approximation. In each trajectory, the z position of the ion was recorded prior to each collision with the background gas. This data was used to generate a histogram of positions. Depending on the conditions, the median position was 2 to 4 mm before the interface between the two modules (Figure 6D). That distance decreased with increasing drift field and/or decreasing applied trap height, but does not appear to be correlated with the effective trap height. The 95% confidence intervals of the positions span <1.5 mm (Figure 6D).

The analysis in the preceding section assumed no contributions from gating (*i.e.*, $w_{gate} = 0$ ms). The effective temporal distribution of ions as the applied trap height is decreased to zero to release ions can be estimated using the spatial distribution of trapped ions along the z axis, K, E, and N. For example, the effective temporal distribution of ions released from a junction trap established using an applied trap height of +12 V and fields of 4, 6, and 8 V cm^{-1} are 330, 160, and 60 μs, respectively. Using a w_{gate} value of 160 μs and diffusion through ^{2}D with a field of 6 V cm^{-1} yields a $w_{conformer}$ value of 1.5 ms, which is very close to the value calculated assuming no contributions from gating. Because this value is still less than the w_{obs} values determined for

372 the corresponding experiments (1.8 ms), this suggests that this analysis is underestimating the
373 w_{gate} in the experiments or that there are additional sources of broadening that have not been
374 included. For example, the spatial distribution of ions in the junction trap may expand as the
375 applied trap height is decreased to zero or the mobility separated ions may experience
376 broadening during transfer through the mass spectrometer.
377
378 *Selection-Only versus Selection-Trapping Tandem Ion Mobility*
379 To compare the results from selection-only and selection-trapping experiments in the
380 context of a structural MS experiment, the data plotted as a function of ^{2}D times in Figure 3 were
381 replotted as a function of apparent Ω in Figure 7. This conversion was made using Equations 1
382 and 2. Even though the $[GRGDS+H]^+$ ions in these experiments are expected to have a single
383 conformation, thus the same *K*, the apparent Ω distributions determined using selection-only
384 experiments depend on the programmed window used for ion selection. The Ω distribution
385 determined using the wider programmed window is not only wider than those determined using
386 the narrower programmed windows, but it is also biased to larger values. This bias was also
387 observed in the ^{2}D time distribution, as discussed earlier, and propagated through the conversion
388 to an apparent Ω distribution. Such artifacts in the apparent Ω distributions, which are
389 characterized here for ions of the same *K*, would make it more challenging to characterize
390 differences between subpopulations of ions with different *K* in future experiments without
391 extensive characterization of the selection process.
392 In contrast, the apparent Ω distributions determined using selection-trapping experiments
393 appear to be independent of the programmed window. That is, the selectively transmitted ions
394 eluting from ^{1}D are spatially focused prior to ^{2}D. This focusing can remove broadening that

occurred during ^{1}D, even when different fractions of the broadened population are filtered away. Therefore, focusing removes the inherent tradeoff between maximizing sensitivity and minimizing w_{gate} that is inherent to selection-only tandem IM experiments, as demonstrated in Figure 4. After focusing, the spatial and kinetic properties of the ions will equilibrate under the conditions of the junction trap; therefore individual ions will lose memory of the spatial and kinetic properties that they had during selection. This process aligns ions that were selected using different timing schemes and establishes common initial conditions prior to ^{2}D. Alignment enables facile and direct comparisons of results between different tandem IM experiments, which will be even more valuable when characterizing differences between subpopulations of ions with different *K*.

Conclusions

Tandem IM enables the independent characterization of subpopulations of ions from larger ensembles. For an instrument operated using selection-only and selection-trapping modes (Figures 1C and 1D), ion transmission, filtering, and focusing were characterized using a combination of experiments and trajectory simulations. In selection-only experiments, decreasing the width of the programmed window that was used to selectively transmit ions eluting from ^{1}D decreases the width of ions eluting from ^{2}D, but at the cost of decreased ion intensity (Figure 4). Additionally, differences between the middle of the programmed window and the middle of the temporal distribution of transmitted ions were observed to bias the ^{2}D times, which can make it more challenging to interpret the results of experiments using different programmed windows (Figures 3A and 7A). Trajectory simulations were used to evaluate the relationship between the programmed window, experimental parameters, and the temporal

418 profile of the ions that are transmitted from ^{1}D to ^{2}D. The actual window of transmitted ions can
419 be very similar to the programmed window, *e.g.*, for programmed windows >300 μs using a
420 collinear drift field of 6 V cm^{-1} and a switch guard bias of +16 V (Figure 5). However, the actual
421 window can vary considerably (±500 μs) depending on the drift field and switch guard bias used
422 for selection.

423 In selection-trapping experiments, ions are briefly trapped between ^{1}D and ^{2}D. The
424 trapped ions are spatially focused prior to ^{2}D, which can remove broadening that occurred during
425 ^{1}D. During focusing, individual ions appear to lose memory of the spatial and kinetic properties
426 that they had during selection, which aligns ions that were selected using different timing
427 schemes and establishes common initial conditions prior to ^{2}D (Figures 3B and 7B). The
428 trajectory simulations suggest that trapped ions are confined in a region along the drift axis
429 spanning ~1.5 mm (Figure 6D). Assuming that ions retain this spatial distribution as they are
430 released into ^{2}D, this would correspond to a narrow temporal distribution (*e.g.*, for ions release
431 from a trap establish using drift field of 6 V cm^{-1} and an applied trap height of +12 V, the
432 effective temporal distribution would be 160 μs, which would be a minor source of broadening in
433 most IM experiments). These results also indicate that trapped ions will be localized 2 to 4 mm
434 prior to where the potentials are applied to establish the trap, which should be accounted for in
435 the drift length used for data analysis.

436 These results will be useful for designing and interpreting the results of future tandem IM
437 experiments. Selection-trapping experiments appear to offer many advantages relative to
438 selection-only experiments. We anticipate that these advantages will become more pronounced
439 in future experiments that will make use of longer IM separations (hence greater diffusion during
440 each dimension) and additional dimensions of analysis.

441

Acknowledgements

This material is based upon work supported by the National Science Foundation under CHE-1807382 (M. F. B.) and DGE-1256082 (R. M. E.) and by the ACS Division of Analytical Chemsitry (fellowship to R. M. E.). We thank Prof. Robert Synovec (University of Washington) for useful discussions. We than Benjamin Zercher (University of Washington) for critically reviewing the manuscript. We thank the SLIM Consortium at Pacific Northwest National Laboratory, including Dr. Richard Smith, Dr. Yehia Ibrahim, Dr. Randy Norheim, Dr. Tsung-Chi Chen, Spencer Prost, and Dr. Ian Webb for sharing designs, software, and technical expertise. We thank Gordon Anderson (GAA Custom Engineering) for assistance with electronics.

Electronic Supplementary Material

The online version of this article contains supplementary material, which is available to authorized users.

References

1. Nyon, M.P., Prentice, T., Day, J., Kirkpatrick, J., Sivalingam, G.N., Levy, G., Haq, I., Irving, J.A., Lomas, D.A., Christodoulou, J., Gooptu, B., Thalassinos, K.: An integrative approach combining ion mobility mass spectrometry, X-ray crystallography, and nuclear magnetic resonance spectroscopy to study the conformational dynamics of α1-antitrypsin upon ligand binding. Protein Sci. 24, 1301–1312 (2015). doi:10.1002/pro.2706
2. Hassell, A.M., An, G., Bledsoe, R.K., Bynum, J.M., Carter, H.L., Deng, S.-J.J., Gampe, R.T., Grisard, T.E., Madauss, K.P., Nolte, R.T., Rocque, W.J., Wang, L., Weaver, K.L., Williams, S.P., Wisely, G.B., Xu, R., Shewchuk, L.M.: Crystallization of protein–ligand complexes. Acta Crystallogr. D Biol. Crystallogr. 63, 72–79 (2007). doi:10.1107/S0907444906047020
3. Leney, A.C., Heck, A.J.R.: Native Mass Spectrometry: What is in the Name? J. Am. Soc. Mass Spectrom. 28, 5–13 (2017). doi:10.1007/s13361-016-1545-3
4. Jore, M.M., Lundgren, M., van Duijn, E., Bultema, J.B., Westra, E.R., Waghmare, S.P., Wiedenheft, B., Pul, Ü., Wurm, R., Wagner, R., Beijer, M.R., Barendregt, A., Zhou, K., Snijders, A.P.L., Dickman, M.J., Doudna, J.A., Boekema, E.J., Heck, A.J.R., van der Oost, J., Brouns, S.J.J.: Structural basis for CRISPR RNA-guided DNA recognition by Cascade. Nat. Struct. Mol. Biol. 18, 529–536 (2011). doi:10.1038/nsmb.2019
5. Hudgins, R.R., Woenckhaus, J., Jarrold, M.F.: High resolution ion mobility measurements for gas phase proteins: correlation between solution phase and gas phase conformations. Int. J. Mass Spectrom. Ion Process. 165–166, 497–507 (1997). doi:10.1016/S0168-1176(97)00182-1

6. Hoffmann, W., von Helden, G., Pagel, K.: Ion mobility-mass spectrometry and orthogonal gas-phase techniques to study amyloid formation and inhibition. Curr. Opin. Struct. Biol. 46, 7–15 (2017). doi:10.1016/j.sbi.2017.03.002
7. Ben-Nissan, G., Sharon, M.: The application of ion-mobility mass spectrometry for structure/function investigation of protein complexes. Curr. Opin. Chem. Biol. 42, 25–33 (2018). doi:10.1016/j.cbpa.2017.10.026
8. Chandler, S.A., Benesch, J.L.: Mass spectrometry beyond the native state. Curr. Opin. Chem. Biol. 42, 130–137 (2018). doi:10.1016/j.cbpa.2017.11.019
9. von Helden, G., Hsu, M.T., Gotts, N., Bowers, M.T.: Carbon cluster cations with up to 84 atoms: structures, formation mechanism, and reactivity. J. Phys. Chem. 97, 8182–8192 (1993). doi:10.1021/j100133a011
10. Clemmer, D.E., Jarrold, M.F.: Ion Mobility Measurements and their Applications to Clusters and Biomolecules. J. Mass Spectrom. 32, 577–592 (1997). doi:10.1002/(SICI)1096-9888(199706)32:6<577::AID-JMS530>3.0.CO;2-4
11. Gabelica, V., Afonso, C., Barran, P.E., Benesch, J.L.P., Bleiholder, C., Bowers, M.T., Bilbao, A., Bush, M.F., Campbell, J.L., D. G. Campuzano, I., Causon, T.J., Clowers, B.H., Creaser, C., De Pauw, E., Far, J., Fernandez-Lima, F., Fjeldsted, J.C., Giles, K., Groessl, M., Hogan, Jr., C.J., Hann, S., Kim, H.I., Kurulugama, R.T., May, J.C., McLean, J.A., Pagel, K., Richardson, K., Ridgeway, M.E., Rosu, F., Sobott, F., Shvartsburg, A.A., Thalassinos, K., Valentine, S.J., Wyttenbach, T.: Recommendations for Reporting Ion Mobility Mass Spectrometry Measurements. Mass Spectrom. Rev. DOI: 10.1002/mas.21585 (2019). doi:10.1002/mas.21585

12. Koeniger, S.L., Merenbloom, S.I., Clemmer, D.E.: Evidence for Many Resolvable Structures within Conformation Types of Electrosprayed Ubiquitin Ions. J. Phys. Chem. B. 110, 7017–7021 (2006). doi:10.1021/jp056165h
13. Allen, S.J., Giles, K., Gilbert, T., Bush, M.F.: Ion mobility mass spectrometry of peptide, protein, and protein complex ions using a radio-frequency confining drift cell. Analyst. 141, 884–891 (2016). doi:10.1039/C5AN02107C
14. Merenbloom, S.I., Koeniger, S.L., Valentine, S.J., Plasencia, M.D., Clemmer, D.E.: IMS−IMS and IMS−IMS−IMS/MS for Separating Peptide and Protein Fragment Ions. Anal. Chem. 78, 2802–2809 (2006). doi:10.1021/ac052208e
15. Li, H., Bendiak, B., Siems, W.F., Gang, D.R., Hill, H.H.: Carbohydrate Structure Characterization by Tandem Ion Mobility Mass Spectrometry (IMMS)^2. Anal. Chem. 85, 2760–2769 (2013). doi:10.1021/ac303273z
16. Adamson, B.D., Coughlan, N.J.A., Markworth, P.B., Continetti, R.E., Bieske, E.J.: An ion mobility mass spectrometer for investigating photoisomerization and photodissociation of molecular ions. Rev. Sci. Instrum. 85, 123109 (2014). doi:10.1063/1.4903753
17. Oberreit, D.R., McMurry, P.H., Hogan, C.J.: Analysis of heterogeneous uptake by nanoparticles via differential mobility analysis–drift tube ion mobility spectrometry. Phys. Chem. Chem. Phys. 16, 6968–6979 (2014). doi:10.1039/C3CP54842B
18. Poyer, S., Comby-Zerbino, C., Choi, C.M., MacAleese, L., Deo, C., Bogliotti, N., Xie, J., Salpin, J.-Y., Dugourd, P., Chirot, F.: Conformational Dynamics in Ion Mobility Data. Anal. Chem. 89, 4230–4237 (2017). doi:10.1021/acs.analchem.7b00281
19. Liu, F.C., Ridgeway, M.E., Park, M.A., Bleiholder, C.: Tandem trapped ion mobility spectrometry. Analyst. 143, 2249–2258 (2018). doi:10.1039/C7AN02054F

20. Ouyang, H., He, S., Larriba-Andaluz, C., Hogan, C.J.: IMS–MS and IMS–IMS Investigation of the Structure and Stability of Dimethylamine-Sulfuric Acid Nanoclusters. J. Phys. Chem. A. 119, 2026–2036 (2015). doi:10.1021/jp512645g
21. Koeniger, S.L., Merenbloom, S.I., Valentine, S.J., Jarrold, M.F., Udseth, H.R., Smith, R.D., Clemmer, D.E.: An IMS−IMS Analogue of MS−MS. Anal. Chem. 78, 4161–4174 (2006). doi:10.1021/ac051060w
22. Dwivedi, P., Schultz, A.J., Jr, H.H.H.: Metabolic profiling of human blood by high-resolution ion mobility mass spectrometry (IM-MS). Int. J. Mass Spectrom. 298, 78–90 (2010). doi:10.1016/j.ijms.2010.02.007
23. Kwantwi-Barima, P., Ouyang, H., Hogan, C.J., Clowers, B.H.: Tuning Mobility Separation Factors of Chemical Warfare Agent Degradation Products via Selective Ion-Neutral Clustering. Anal. Chem. 89, 12416–12424 (2017). doi:10.1021/acs.analchem.7b03518
24. Simon, A.-L., Chirot, F., Choi, C.M., Clavier, C., Barbaire, M., Maurelli, J., Dagany, X., MacAleese, L., Dugourd, P.: Tandem ion mobility spectrometry coupled to laser excitation. Rev. Sci. Instrum. 86, 094101 (2015). doi:10.1063/1.4930604
25. Allen, S.J., Eaton, R.M., Bush, M.F.: Structural Dynamics of Native-Like Ions in the Gas Phase: Results from Tandem Ion Mobility of Cytochrome *c*. Anal. Chem. 89, 7527–7534 (2017). doi:10.1021/acs.analchem.7b01234
26. Pierson, N.A., Valentine, S.J., Clemmer, D.E.: Evidence for a Quasi-Equilibrium Distribution of States for Bradykinin [M + 3H]3+ Ions in the Gas Phase. J. Phys. Chem. B. 114, 7777–7783 (2010). doi:10.1021/jp102478k

27. Koeniger, S.L., Clemmer, D.E.: Resolution and Structural Transitions of Elongated States of Ubiquitin. J. Am. Soc. Mass Spectrom. 18, 322–331 (2007). doi:10.1016/j.jasms.2006.09.025
28. Ibrahim, Y.M., Hamid, A.M., Deng, L., Garimella, S.V.B., Webb, I.K., Baker, E.S., Smith, R.D.: New frontiers for mass spectrometry based upon structures for lossless ion manipulations. Analyst. 142, 1010–1021 (2017). doi:10.1039/C7AN00031F
29. Garimella, S.V.B., Ibrahim, Y.M., Webb, I.K., Tolmachev, A.V., Zhang, X., Prost, S.A., Anderson, G.A., Smith, R.D.: Simulation of Electric Potentials and Ion Motion in Planar Electrode Structures for Lossless Ion Manipulations (SLIM). J. Am. Soc. Mass Spectrom. 25, 1890–1896 (2014). doi:10.1007/s13361-014-0976-y
30. Webb, I.K., Garimella, S.V.B., Tolmachev, A.V., Chen, T.-C., Zhang, X., Norheim, R.V., Prost, S.A., LaMarche, B., Anderson, G.A., Ibrahim, Y.M., Smith, R.D.: Experimental Evaluation and Optimization of Structures for Lossless Ion Manipulations for Ion Mobility Spectrometry with Time-of-Flight Mass Spectrometry. Anal. Chem. 86, 9169–9176 (2014). doi:10.1021/ac502055e
31. Tolmachev, A.V., Webb, I.K., Ibrahim, Y.M., Garimella, S.V.B., Zhang, X., Anderson, G.A., Smith, R.D.: Characterization of Ion Dynamics in Structures for Lossless Ion Manipulations. Anal. Chem. 86, 9162–9168 (2014). doi:10.1021/ac502054p
32. Allen, S.J., Bush, M.F.: Radio-Frequency (RF) Confinement in Ion Mobility Mass Spectrometry: Apparent Mobilities and Effective Temperatures. J. Am. Soc. Mass Spectrom. 27, 2054–2063 (2016). doi:10.1007/s13361-016-1479-9

33. Allen, S.J., Eaton, R.M., Bush, M.F.: Analysis of Native-Like Ions Using Structures for Lossless Ion Manipulations. Anal. Chem. 88, 9118–9126 (2016). doi:10.1021/acs.analchem.6b02089

34. Webb, I.K., Garimella, S.V.B., Tolmachev, A.V., Chen, T.-C., Zhang, X., Cox, J.T., Norheim, R.V., Prost, S.A., LaMarche, B., Anderson, G.A., Ibrahim, Y.M., Smith, R.D.: Mobility-Resolved Ion Selection in Uniform Drift Field Ion Mobility Spectrometry/Mass Spectrometry: Dynamic Switching in Structures for Lossless Ion Manipulations. Anal. Chem. 86, 9632–9637 (2014). doi:10.1021/ac502139e

35. Chen, T.-C., Ibrahim, Y.M., Webb, I.K., Garimella, S.V.B., Zhang, X., Hamid, A.M., Deng, L., Karnesky, W.E., Prost, S.A., Sandoval, J.A., Norheim, R.V., Anderson, G.A., Tolmachev, A.V., Baker, E.S., Smith, R.D.: Mobility-Selected Ion Trapping and Enrichment Using Structures for Lossless Ion Manipulations. Anal. Chem. 88, 1728–1733 (2016). doi:10.1021/acs.analchem.5b03910

36. Zhang, X., Garimella, S.V.B., Prost, S.A., Webb, I.K., Chen, T.-C., Tang, K., Tolmachev, A.V., Norheim, R.V., Baker, E.S., Anderson, G.A., Ibrahim, Y.M., Smith, R.D.: Ion Trapping, Storage, and Ejection in Structures for Lossless Ion Manipulations. Anal. Chem. 87, 6010–6016 (2015). doi:10.1021/acs.analchem.5b00214

37. Davidson, K.L., Oberreit, D.R., Hogan, C.J., Bush, M.F.: Nonspecific aggregation in native electrokinetic nanoelectrospray ionization. Int. J. Mass Spectrom. 420, 35–42 (2017). doi:10.1016/j.ijms.2016.09.013

38. Clowers, B.H., Ibrahim, Y.M., Prior, D.C., Danielson, W.F., Belov, M.E., Smith, R.D.: Enhanced Ion Utilization Efficiency Using an Electrodynamic Ion Funnel Trap as an

Injection Mechanism for Ion Mobility Spectrometry. Anal. Chem. 80, 612–623 (2008). doi:10.1021/ac701648p

39. Chen, T.-C., Webb, I.K., Prost, S.A., Harrer, M.B., Norheim, R.V., Tang, K., Ibrahim, Y.M., Smith, R.D.: Rectangular Ion Funnel: A New Ion Funnel Interface for Structures for Lossless Ion Manipulations. Anal. Chem. 87, 716–722 (2015). doi:10.1021/ac503564c

40. Shaffer, S.A., Tolmachev, A., Prior, D.C., Anderson, G.A., Udseth, H.R., Smith, R.D.: Characterization of an Improved Electrodynamic Ion Funnel Interface for Electrospray Ionization Mass Spectrometry. Anal. Chem. 71, 2957–2964 (1999). doi:10.1021/ac990346w

41. Ibrahim, Y.M., Baker, E.S., Danielson III, W.F., Norheim, R.V., Prior, D.C., Anderson, G.A., Belov, M.E., Smith, R.D.: Development of a new ion mobility time-of-flight mass spectrometer. Int. J. Mass Spectrom. 377, 655–662 (2015). doi:10.1016/j.ijms.2014.07.034

42. Garimella, S.V.B., Ibrahim, Y.M., Webb, I.K., Ipsen, A.B., Chen, T.-C., Tolmachev, A.V., Baker, E.S., Anderson, G.A., Smith, R.D.: Ion manipulations in structures for lossless ion manipulations (SLIM): computational evaluation of a 90° turn and a switch. Analyst. 140, 6845–6852 (2015). doi:10.1039/C5AN00844A

43. Watson, N.E., Bahaghighat, H.D., Cui, K., Synovec, R.E.: Comprehensive Three-Dimensional Gas Chromatography with Time-of-Flight Mass Spectrometry. Anal. Chem. 89, 1793–1800 (2017). doi:10.1021/acs.analchem.6b04112

44. Mason, E.A., McDaniel, E.W.: Transport Properties of Ions in Gases. Wiley, New York (1988)

45. Dahl, D.: SIMION. SIMION. version 8.1; Idaho National Engineering Laboratory: Idaho Falls, ID.

46. Bush, M.F., Hall, Z., Giles, K., Hoyes, J., Robinson, C.V., Ruotolo, B.T.: Collision Cross Sections of Proteins and Their Complexes: A Calibration Framework and Database for Gas-Phase Structural Biology. Anal Chem. 82, 9557–9565 (2010). doi:10.1021/ac1022953

47. Kanu, A.B., Gribb, M.M., Hill, H.H.: Predicting Optimal Resolving Power for Ambient Pressure Ion Mobility Spectrometry. Anal. Chem. 80, 6610–6619 (2008). doi:10.1021/ac8008143

48. Davidson, K.L., Bush, M.F.: Effects of Drift Gas Selection on the Ambient-Temperature, Ion Mobility Mass Spectrometry Analysis of Amino Acids. Anal. Chem. 89, 2017–2023 (2017). doi:10.1021/acs.analchem.6b04605

Table 1. Summary of Programmed Windows, Drift Time Distributions, and Ω Distributions.

	Unit	Selection-Only			Selection-Trapping		
$t_{transmit}$	ms	32.000	33.250	34.625	32.000	33.250	34.625
t_{divert}	ms	36.375	33.750	35.125	36.375	33.750	35.125
Programmed Window	ms	4.375	0.500	0.500	4.375	0.500	0.500
^{2}D time	ms	23.0	22.8	22.8	20.1	20.0	20.1
w_{obs}	ms	3.5	1.8	1.8	1.8	1.7	1.8
$w_{conformer}$	ms	3.0	1.8	1.8	1.5	1.5	1.5
Ω	nm^2	2.06	2.04	2.03	2.06	2.05	2.05
w_{obs}	nm^2	0.48	0.25	0.25	0.30	0.28	0.31
$w_{conformer}$	nm^2	0.41	0.25	0.25	0.25	0.25	0.25

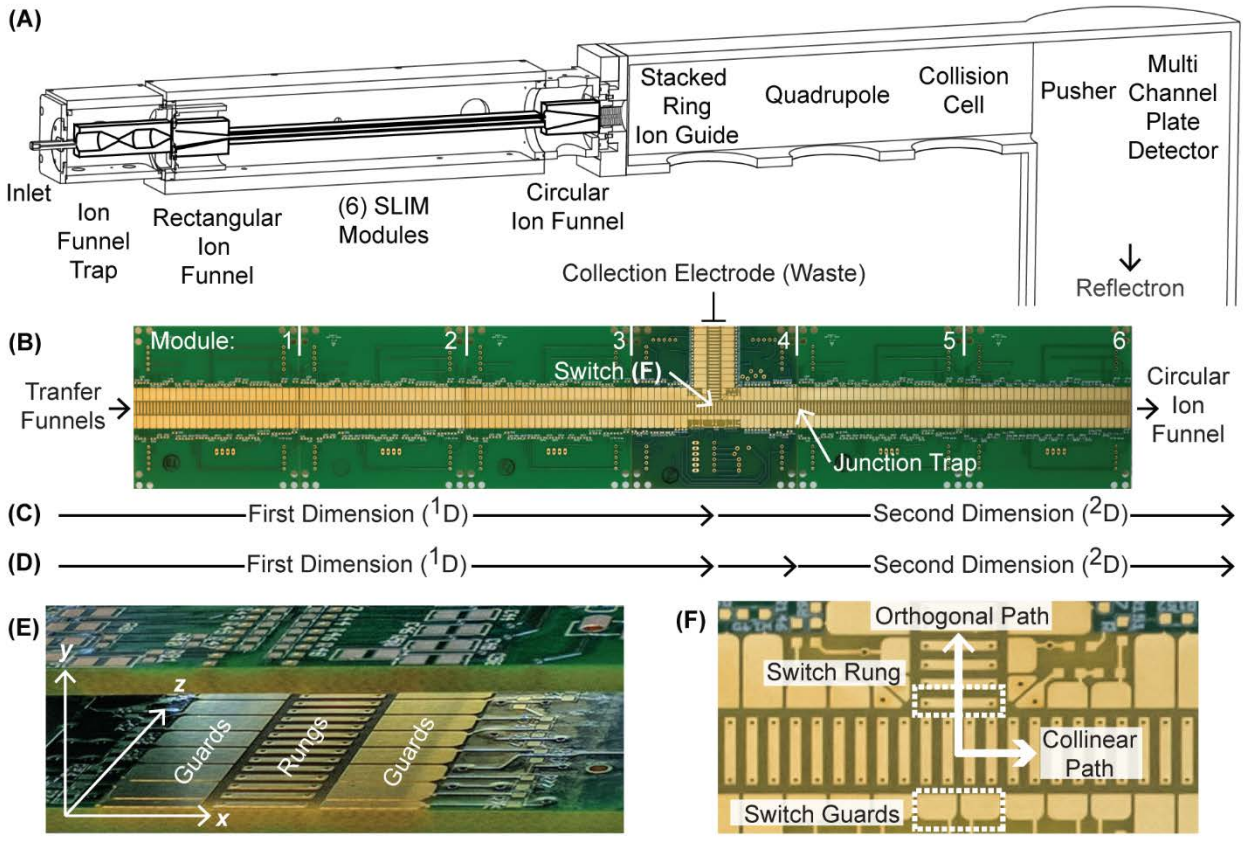

Figure 1. (A) Drawing of the hybrid instrument, which has been described previously [25, 33]. (B) Photograph of the array of SLIM modules used for these experiments, with the top board of each module removed. (C) In selection-only tandem IM experiments, ions are first separated during transport from the transfer funnels (post-trapping region of the ion funnel trap and the rectangular ion funnel) to the switch on module 4, which selectively transmits ions of interest that are then separated further during transport to mass spectrometer. (D) In selection-trapping tandem IM experiments, ions selected at the switch region are transferred to the junction trap, which is established by biasing the DC potentials between modules 4 and 5. After a delay, the trapped ions are released and separated during transport to mass spectrometer. (E) Side view of a module, showing the coordinate system as well as the guard and rung electrodes. (F) Photograph of the region near the switch, showing the electrodes that are controlled to direct ions to the collinear or orthogonal paths.

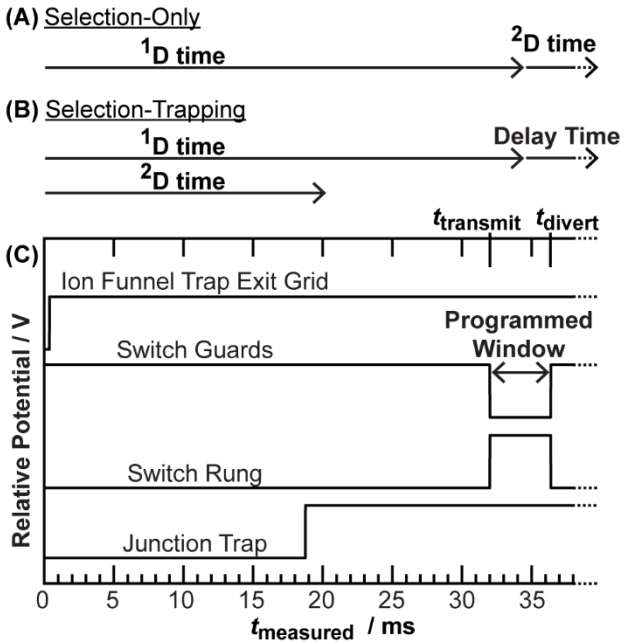

Figure 2. Representative residence times for ions in (A) selection-only and (B) selection-trapping, as well as (C) representative potentials of selected electrodes during $[GRGDS+H]^+$ experiments. Both the ion funnel trap and the junction trap were programmed to release ions when $t_{measured}$ = 0 ms. In selection-only mode, $t_{measured}$ is the drift time through both ^1D and ^2D, while in selection-trapping mode $t_{measured}$ monitors the drift time through ^2D. The programmed window used to selectively transmit ions depends on the time points ($t_{transmit}$ and t_{divert}) when the relative potentials of the switch guard and rung electrodes were modulated. The delay time is defined as the average time of $t_{transmit}$ and t_{divert} until the release of the junction trap.

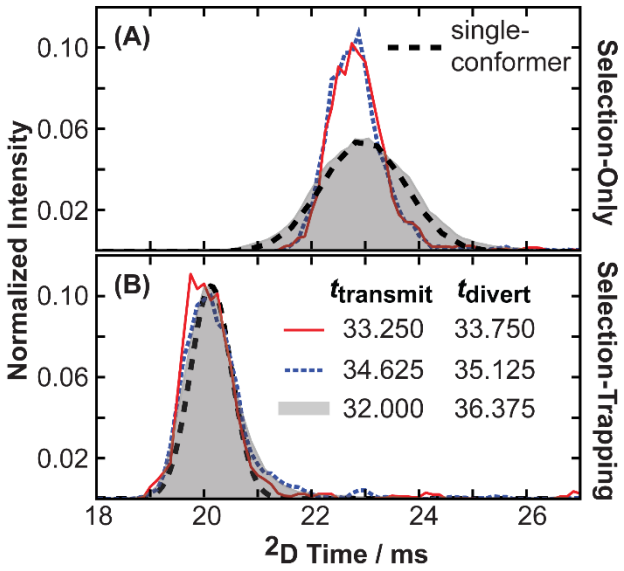

Figure 3. ^{2}D time distributions determined using (A) selection-only and (B) selection-trapping analysis of $[GRGDS+H]^+$, based on experiments performed using a 6 V cm^{-1} drift field and 4.0 Torr N_2. For both modes, the entire population was isolated using a programmed window from 32.000 to 36.375 ms (*shaded distribution*). Two subpopulations were isolated using programmed windows from 33.250 to 33.750 ms (*solid red trace*) or 34.625 to 35.125 ms (*dashed blue trace*). In the selection-trapping experiments, the applied trap height was +12 V. For comparison, the expected distribution for a single conformer of $[GRGDS+H]^+$ was calculated and is shown using a *black dashed line*.

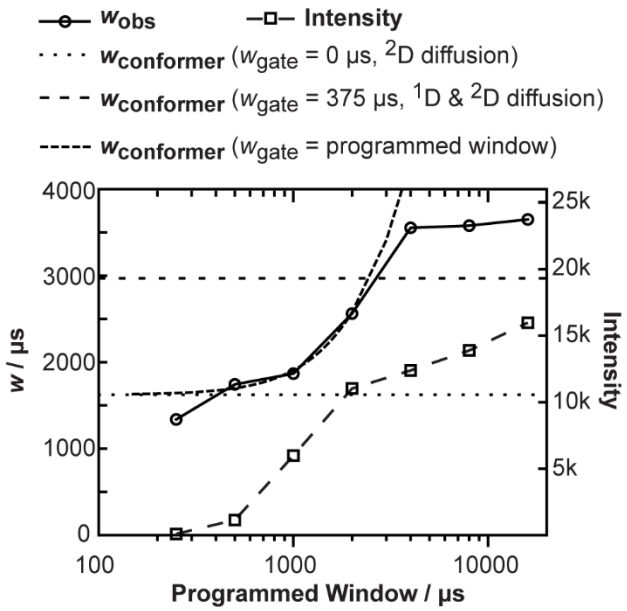

Figure 4. Results from the selection-only analysis of $[GRGDS+H]^+$ performed using a 6 V cm^{-1} drift field and a switch guard voltage of +16 V relative to the switch region. The observed width at base (w_{obs}, *circles*) is similar to that expected for a single conformer ($w_{conformer}$, heavy dashed line) estimated using Equation 3 and assuming that w_{gate} equals the programmed window. The expected width at base from diffusion (*short dotted line*) shows the diminishing contribution of diffusion as the programmed window is increased. The expected width at base for a single conformer with a w_{gate} from the ion funnel trap (w_{gate} = 375 µs) and diffusion through ^{1}D and ^{2}D ($w_{conformer}$, *light dashed line*) is also plotted. The ion intensity (*squares*) is plotted on the right vertical axis. For all experiments, the switch guards and switch rung were set to +11 V relative to the switch region to transmit ions along the collinear path. To divert ions down the orthogonal path, the switch rung was set to 0 V and switch guard set to +16 V relative to the switch region.

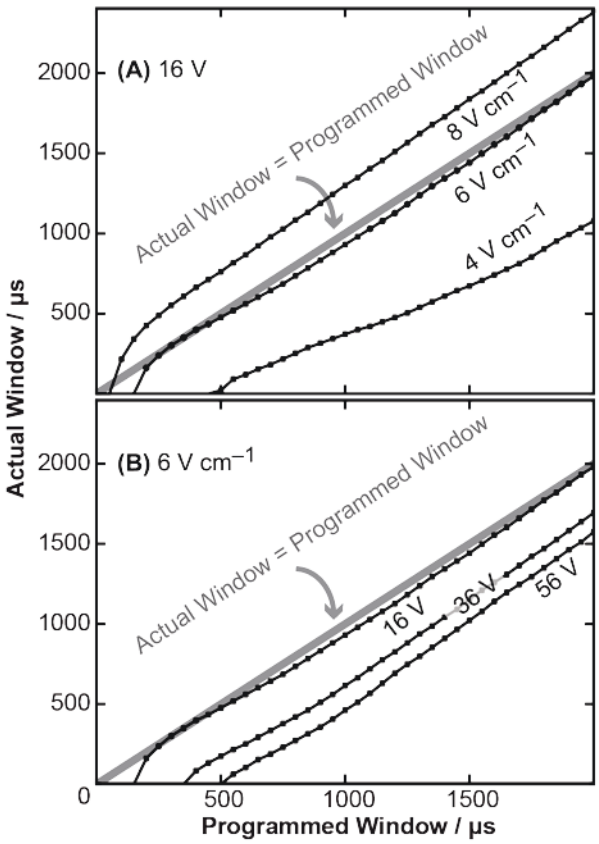

Figure 5. Results from a series of ion trajectory simulations performed as a function of the duration of the programmed window under either (A) varying collinear drift field with a switch guard bias of +16 V or (B) varying switch guard bias with a collinear drift field of 6 V cm^{-1}. The actual window is determined from the range of starting positions that results in transmission along the collinear path, as shown in Figure S1. During the programmed window for each simulation, the switch guards and rung were set to +11 V relative to the switch region to transmit ions along the collinear path.

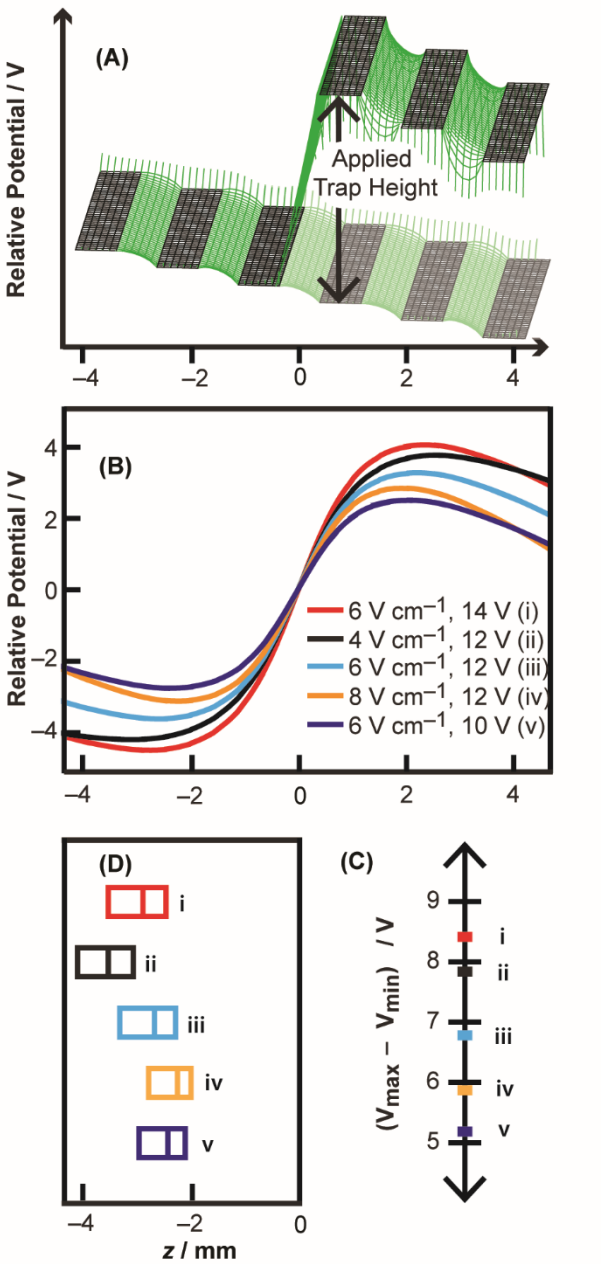

Figure 6. (A) DC potentials at the surface of the boards near the interface between modules 4 and 5 used to create a junction trap. The interface of modules 4 and 5 is defined as 0 mm along the *z* axis. The DC potential (B) and the effective trap height, defined as the difference between the local minimum and local maximum of the DC potential (C), along the axis of transmission. (D) Box plot representations of the median and 95% confidence interval of the *z*-axis positions of a $[GRGDS+H]^+$ ion stored in the junction trap.

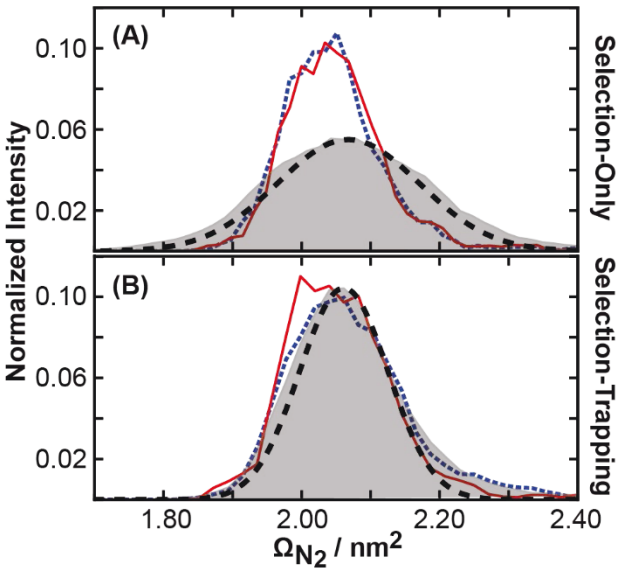

Figure 7. Apparent Ω distributions of $[GRGDS+H]^+$ ions that were determined from the ^2D time distributions in Figure 3, the conditions of the experiment, and Equations 1 and 2. For both selection-only and selection-trapping experiments, the entire population was isolated using a programmed window from 32.000 to 36.375 ms (*shaded distribution*). Two subpopulations were isolated using programmed windows from 33.250 to 33.750 ms (*solid red trace*) or 34.625 to 35.125 ms (*dashed blue trace*). In the selection-trapping experiments, the applied trap height was +12 V. For comparison, the expected distribution for a single conformer was calculated and is shown using a *black dashed line*.

Principles of Ion Selection, Alignment, and Focusing in Tandem Ion Mobility Implemented Using Structures for Lossless Ion Manipulations (SLIM)

*Rachel M. Eaton, Samuel J. Allen, Matthew F. Bush**

ELECTRONIC SUPPLEMENTARY MATERIAL

Contribution from the:

University of Washington, Department of Chemistry, Box 351700

Seattle, WA 98195-1700

*Address correspondence to mattbush@uw.edu

Table S1 ..... S-2

Figure S1 ..... S-3

Figure S2 ..... S-4

Figure S3 ..... S-5

Table S1. Drift Voltages, Expected Drift Time, and Expected Widths for Single-Conformer $[GRGDS+H]^+$ Ions Transported Through Instrument.

	Unit	Post-trap, Ion Funnel Trap	Rectangular Ion Funnel	6 SLIM Modules	Circular Ion Funnel
Applied Drift Voltage[a]	V	37.3	30.6	271	37.4
Expected Drift Time	ms	0.899	11.6	36.8	6.47
Expected $w_{diffusion}$	ms	0.134	1.90	2.2	0.963

[a] Using a drift field of 6 V cm^{-1}.

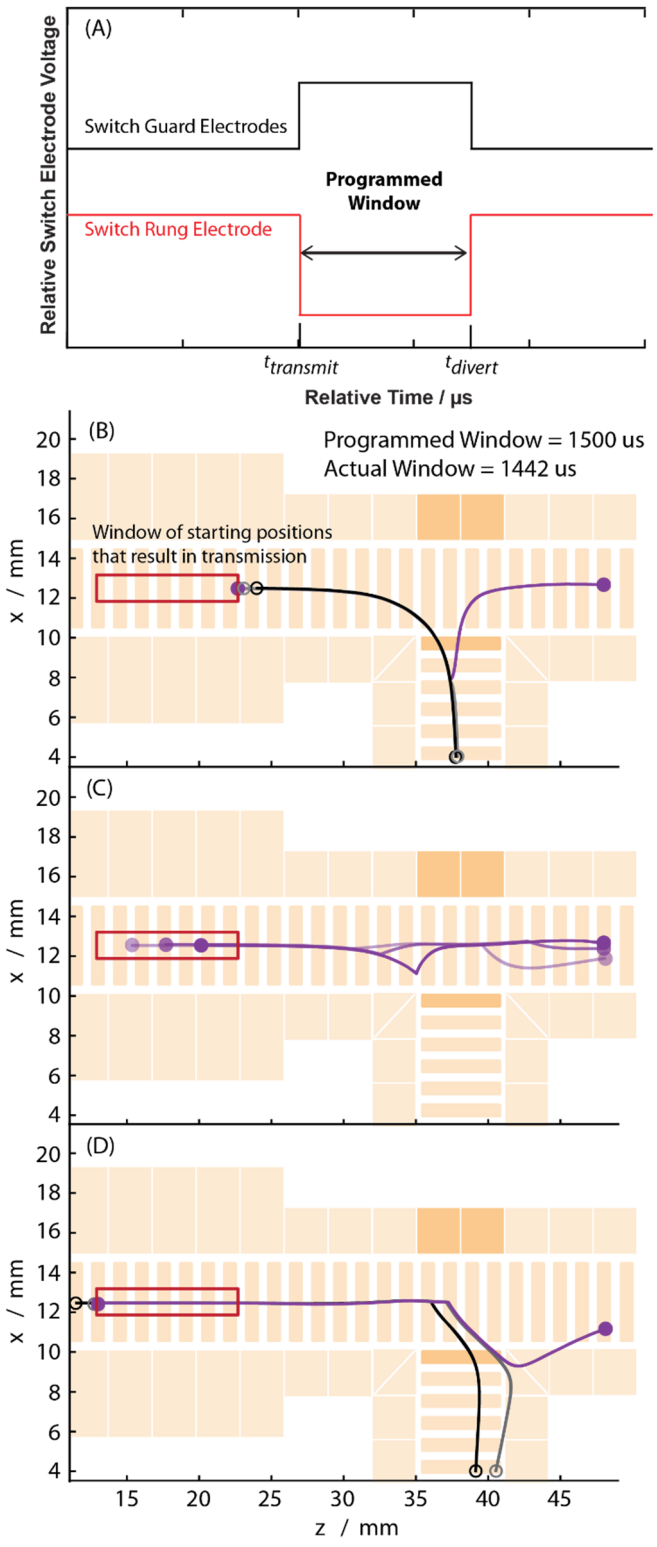

Figure S1. Representative trajectories used to probe the actual transmission window of $[GRGDS+H]^+$. These simulations use a programmed window of 1500 µs, a collinear drift field of 6 V cm^{-1}, and a +16 V switch guard bias. (A) Modulation of switch guard and switch rung electrode potentials used in ion selection simulations. The $t_{transmit}$ was kept constant for all trajectories at a given drift field (drift fields of 4, 6, and 8 V cm^{-1} had $t_{transmit}$ values of 2500, 2000, and 1000 µs, respectively) while t_{divert} was changed to achieve the desired programmed window. Starting positions are shown for ion trajectories that arrive in the switch region (B) when the programmed window begins or (C) during the programmed window, or that are (D) within the switch region at the end of the programmed window. The red box in each image spans the starting positions that will result in transmission. The tan boxes map the electrode surface found in the vicinity of the switch region; the orange squares and rectangle are the switch guard electrodes and the switch rung electrode, respectively.

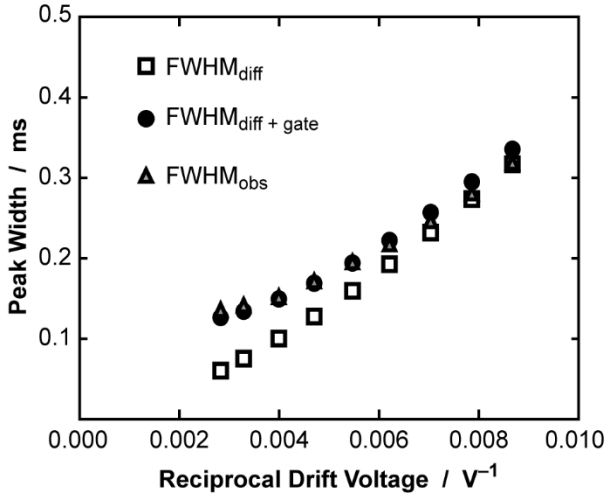

Figure S2. Peak width as a function of reciprocal drift voltage for $[GRGDS+H]^+$ determined using an RF-confining drift cell operated at 1.006 Torr nitrogen gas. Observed experimental peak widths ($FWHM_{obs}$, *triangles*) plotted with the values expected based only on diffusion ($FWHM_{diff}$, *squares*) and based on gating and diffusion ($FWHM_{diff+gate}$, *circles*).

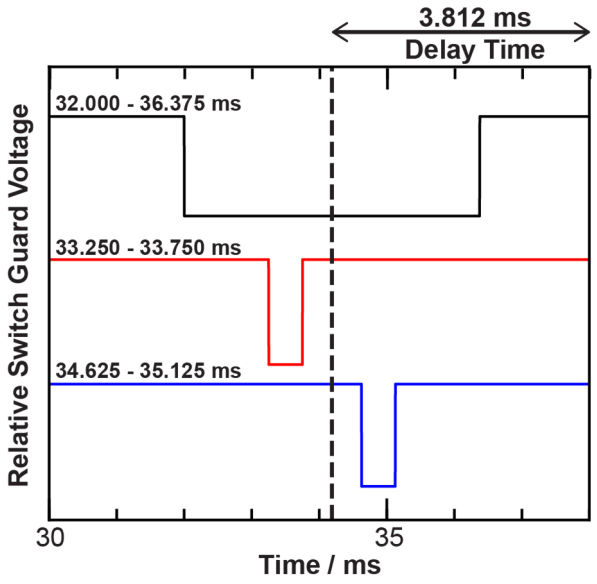

Figure S3. Relative voltage applied to the switch guards during the selection-trapping experiments in Figures 3 and 7. For simplicity, a common delay time of 3.812 ms is used to describe the time between the first and second IM dimension. Note, the switch rung voltage (not shown) is also modulated using these same times.